Synthetic aperture superresolution with multiple off-axis holograms

Vicente Mico

AIDO, Technological Institute of Optics, Colour and Imaging, C/. Nicolás Copérnico, 7-13 Parc Tecnològic, 46980 Paterna (Valencia), Spain

Zeev Zalevsky

School of Engineering, Bar-Ilan University, Ramat-Gan, 52900 Israel

Pascuala García-Martínez and Javier García

Departamento de Óptica, Universitat de València, C/. Dr. Moliner, 50, 46100 Burjassot, Spain

Received February 27, 2006; revised June 13, 2006; accepted June 30, 2006; posted July 5, 2006 (Doc. ID 68449)

An optical setup to achieve superresolution in microscopy using holographic recording is presented. The technique is based on off-axis illumination of the object and a simple optical image processing stage after the imaging system for the interferometric recording process. The superresolution effect can be obtained either in one step by combining a spatial multiplexing process and an incoherent addition of different holograms or it can be implemented sequentially. Each hologram holds the information of each different frequency bandpass of the object spectrum. We have optically implemented the approach for a low-numerical-aperture commercial microscope objective. The system is simple and robust because the holographic interferometric recording setup is done after the imaging lens. © 2006 Optical Society of America

OCIS codes: 090.0090, 100.6640, 110.0180.

1. INTRODUCTION

Digital holography permits reconstruction of both amplitude and phase of imaged objects. The amplitude distribution of the imaging beam is added in the hologram plane with a reference wave and the hologram is recorded by using a CCD camera. Then the object wavefront is reconstructed numerically by simulating the backpropagation of the complex amplitude of the optical beam using the Kirchhoff–Fresnel propagation equations.[1–4] However, for both off-axis[4] and on-axis[5] holography, the finite number of recorded pixels and the size of the CCD limit the resolution of the digital holographic approach. Some techniques have been proposed in the past to overcome this limitation. One can classify them into two groups: phase-shifting digital holography (PSDH) techniques and holographic synthetic aperture generation methods.

PSDH uses both an in-line setup to decrease the fringe spacing and a phase shifting of the reference beam to evaluate directly the complex amplitude at the CCD plane and to eliminate the conjugate images completely.[6,7] PSDH has also been applied to three-dimensional microscopy,[8,9] encryption,[10] and wavefront reconstruction.[11] PSDH improves the number of resolved object points contained in the final image by approximately a factor of 2 in comparison with conventional digital holography.

A significant resolution improvement is obtained using holographic synthetic aperture methods. Some of these methods are based on the generation of a synthetic aperture by combining different holograms recorded at different camera positions to construct a larger digital hologram.[12,13] The resolution improvement factor is equal to the number of recorded holograms. Other approaches to generate synthetic apertures are based on superresolution techniques.[14–25] A synthetic enlargement of the system aperture is a well-known and widely used technique[16,20,21] to improve the limited resolving power of optical systems. Because of the wave nature of light, each optical imaging system is limited in resolution linked to a low-pass filtering in the frequency space. The cutoff frequency in the spatial-frequency domain is defined in terms of its numerical aperture (NA) and the wavelength of the illumination light. One can realize that both improving the NA of the imaging system and/or decreasing the wavelength result in a resolution enhancement of the optical system. But in many cases these options are difficult, complex, and not always possible to achieve. Thus, the basis of superresolution is to produce a synthetic enlargement in the system aperture without changing the physical dimensions of the lenses or the illumination wavelength.

Many attempts had been proposed over the years for superresolution imaging based on a certain *a priori* knowledge about the object as its time,[20–22] polarization,[23,24] or wavelength independence.[25] All of these parameters are involved in the information capacity theory,[16,17,19] which gives an invariance theorem for the number of degrees of freedom of an optical system. This theorem states that it is not the spatial bandwidth but the information capacity of an imaging system that re-

1084-7529/06/123162-9/$15.00

mains constant. Thus, it is possible to extend the spatial bandwidth by encoding or decoding the additional information onto unused parameters of the imaging system.

In the past years, Chen and Brueck[26] and Schwarz *et al.*[27] have implemented an interferometric approach applied to lithography and microscopy imaging, respectively. They used off-axis illumination to downshift the high-frequency components of the object spectrum in such a way that they are transmitted through the system aperture. Then, by means of an optical interferometric recording, these transmitted components are shifted back toward their original position at the object spectrum and a synthetic enlargement of the system aperture is done by incoherent addition of the individual recorded intensities. Mico *et al.*[28] obtained the same effect of incoherent addition by using an array of mutually incoherent light sources [a vertical-cavity surface-emitting laser (VCSEL) array] for recording all the spatial-frequency bands in a Mach–Zenhder interferometric configuration. In contrast to the setups reported in Refs. 26 and 27, the transmission of all the spatial frequencies is done at once, in terms of spatial multiplexing of all the incoherent illumination sources. In the method of Mico *et al.*,[28] a large factor of improvement is obtained without penalty for the complexity of the system. In fact, the authors have used five sources simultaneously (fivefold increase of the system spatial-frequency bandwidth) as compared with the three illumination sources for the system presented in Refs. 26 and 27.

Although other authors have implemented incoherent illumination sources to increase the resolution of optical imaging systems,[29,30] the approach presented in Ref. 28 provides higher light efficiency due to the high optical power of the VCSEL array. Moreover, no theoretical limit regarding the limited size of the extended incoherent source restricts the system because of the great number of single VCSELs that can be present in the VCSEL array. In addition, the fact that the VCSEL elements can be temporally modulated up to several gigahertz implies that any synthetic transfer function can be synthesized by temporally varying the relative amplitudes of each source in the array. This can be done because the synthetic aperture generated by the suggested approach[28] is a convolution operation between the VCSEL line array and the coherent transfer function (CTF) of the system.

Recently, Mico *et al.*[31] have extended the optical system of Ref. 28 to two-dimensional (2D) objects. However, the main disadvantage of this setup is that, owing to the difference between the imaging and the reference arm in the interferometer, the holograms for the different bandpasses are incorrectly overlapped, and so it impedes the recording of all frequency slots in a single exposure. Moreover, the stability of the system, as well as that for Ref. 28, suffers from the splitting of light for the reference beam before illuminating the object.

In this paper we present a new experimental configuration that significantly increases the robustness of the system as well as opens the possibility of performing the imaging with enhanced resolution in a single exposure. The system uses a collection of mutually incoherent point sources, at different lateral positions, which serve as spherical and tilted illuminations for the object (i.e., every point source gives a spherical wave with a different origin). The imaging and reference beams are separated by a beam splitter (BS) after the low-NA microscope lens. Therefore, the full interferometer is after the lens, reducing the sensitivity of the system to vibrations and/or thermal changes. One of the arms is filtered using a pinhole array so that the dc of each tilted illumination beam is selected and in addition serves as the set of tilted reference beams. With this new optical system the frequency slots of the spectrum of the superresolved image can be separated, in contrast with the system shown in Ref. 31. Thus, the superresolution system can be implemented by means of a physical 2D array of sources (such as a VCSEL array) in a single exposure. However, as an alternative to the VCSEL array, the implementation can be made sequentially displacing a single coherent source and recording a set of exposures for a later digital combination.

The paper is organized as follows: Sections 2 and 3 give a preliminary and theoretical analysis of the experimental setup, respectively. In Section 4 experimental results and the reconstruction process are presented. Section 5 concludes the paper.

2. PRESENTED APPROACH: SOME SYSTEM CONSIDERATIONS

The optical setup is shown in Fig. 1. The input object is illuminated by a collection of spherical waves, each one coming from different point sources in a 2D array configuration. A microscope objective images the object onto a CCD. Behind the microscope objective, the first beam splitter (BS1) splits the imaging beam into two beams. One of them (right branch in Fig. 1) allows image formation of the object onto the CCD after reflection in mirror M1. We call this branch as imaging arm. In the other optical beam path (left branch in Fig. 1), some elements are introduced to perform optical image processing. This branch is called the reference arm. In the following we explain in detail the configuration of the reference arm in this new superresolution technique.

Diffraction theory applied to optical imaging shows that the object spectrum (Fourier transformation of the object amplitude distribution) is obtained in the image plane of the illumination source through the imaging optical system. In the on-axis illumination case, a pinhole placed at the Fourier plane in the center of the reference arm, coinciding at the axial position of the source image, will transmit only radiation representing the dc term. This procedure gives a uniform reference beam that can be used to perform the interferometric recording in the CCD plane.

When off-axis illumination is used, the full object spectrum is displaced at the Fourier plane and the zero frequency no longer coincides with the pinhole location and, in general, the amount of light passing the pinhole will be negligible. To optimize the intensity of the filtered reference beam, the transmission of the central part in the object spectrum can be performed by moving the pinhole to the off-axis position defined by the object spectrum center. The same effect can be obtained using a mask with an array of pinholes when a certain off-axis illumination configuration is given, instead of shifting a single pinhole.

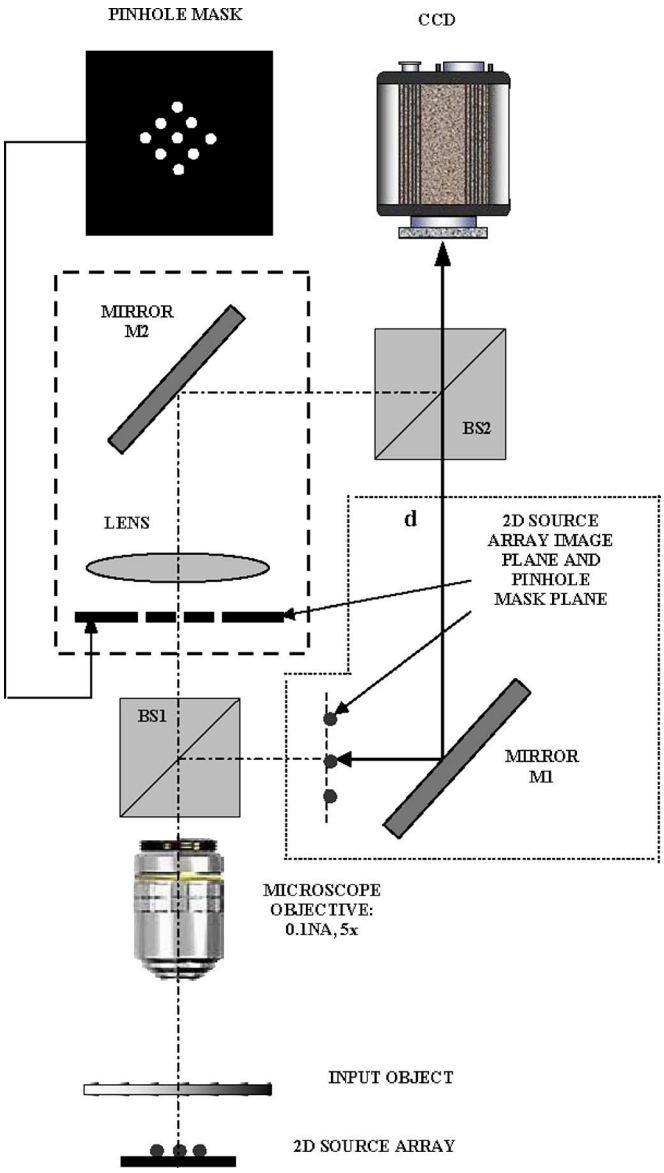

Fig. 1. (Color online) Experimental setup. The reference and imaging arms are marked with dashed and dotted frames, respectively. The divergence distance d for the illumination in the imaging arm is depicted by broken segments ending in arrows.

This pinhole mask must have a pinhole corresponding to each of the 2D illumination point-source arrays. The location of each pinhole is determined by the magnification of the microscope objective (see Fig. 1). Thus, for the case of VCSEL source illumination, if several off-axis sources are operated at the same time, the previously described pinhole mask placed at the Fourier plane will transmit in parallel each of the reference beams corresponding to the different replicas of the object spectrum transmitted by the imaging system.

It is important to note that the input object could be illuminated by off-axis illumination angles higher than that defined by the NA of the microscope objective.[30,32] As a general rule, we can say that the simpler the lens, the higher the off-axis illumination angle. A resolution improvement by a factor of 2 is always achievable using off-axis illumination with a maximum illumination angle equal to the NA of the imaging lens and a postprocessing stage.[31,33] But in our case, when a low-NA objective microscope is used (that means a simpler lens system in comparison with higher-NA objectives), a resolution improvement factor higher than 2 is possible. In fact, for the setup presented in this paper, the resolution improvement factor is 3.

Assuming mutually incoherent point sources, each transmitted reference beam is coherent with its corresponding frequency band transmitted by the imaging arm and incoherent with the others. This property permits the recording process of different frequency bands at the same instant by mixing both the reference and the imaging beams using a second beam splitter (BS2). Moreover, each filtered reference beam has a slightly different car-

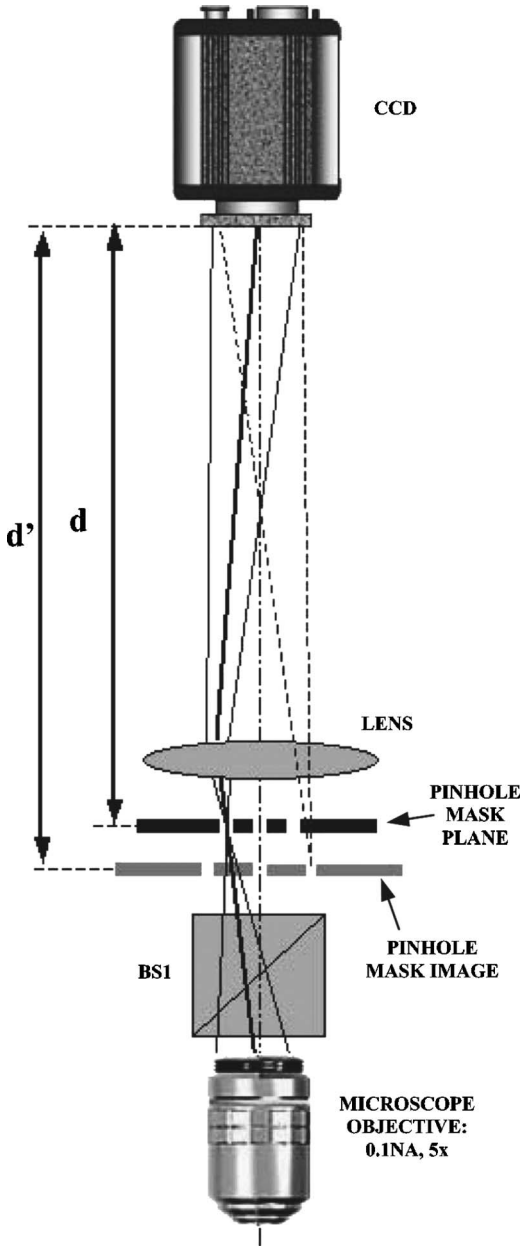

Fig. 2. Off-axis illumination case. The chief ray for each off-axis source (thick solid line) impinges on the CCD center. An approximate size and location of the virtual image of the pinhole mask are shown.

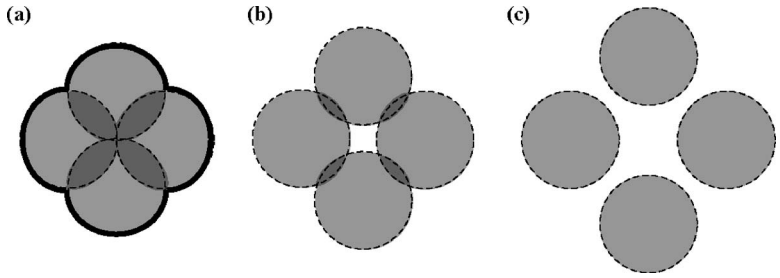

Fig. 3. Lens selection process: (a) Synthetic aperture generated without the field lens (correct overlapping), (b) incorrect overlapping of the different frequency bands (reconstruction is not possible), (c) separated frequency bands obtained using a suitable lens that permits the separated processing of the frequency bands and correct relocation to obtain the desired synthetic aperture shown in (a).

rier frequency that shifts back the corresponding frequency band to its original position in the object spectrum. A bias frequency is introduced by tilting mirrors M1 or M2 to avoid the overlapping of the hologram diffraction orders with the dc term. Simple digital postprocessing is performed to obtain the reconstruction. This digital postprocessing involves an inverse Fourier transformation of the recorded multiple hologram, a filtering and centering process of the first diffraction hologram order, and finally a direct Fourier transformation of the previous centered spectrum.

For the previously mentioned system, the recording of the hologram at the CCD requires long integration times due to the low intensity in the reference beams, owing to their divergence and angular shift. To eliminate this effect, a lens is placed in the reference arm (see Fig. 1). The purpose of this lens is to redirect the light from each reference beam onto the CCD, allowing a more efficient holographic recording (Fig. 2). In the ideal case, the lens is placed at the same plane as the pinhole mask, acting as a field lens. For this purpose, the focal length of the lens is chosen so that the image of the exit pupil of the microscope objective lies on the CCD. Under this condition, the chief rays for every source (and therefore the reference beams) are centered on the CCD. The position of the pinhole array through the field lens is not affected. Thus, the carrier frequency of the holograms for each source is the same as it would be without the lens, providing the proper overlapping of the frequency bands [see Fig. 3(a)].

For a real situation the field lens cannot be attached to the pinhole mask, but an axial displacement is needed. The effect of the lens can be easily interpreted considering the image of the pinhole mask through this lens. The image is virtual and it is located prior to the original mask position and with lateral magnification (Fig. 2). The axial shift of the pinhole array image implies a different curvature of the reference and the imaging beams (associated with divergence distances d and d' shown in Figs. 1 and 2, respectively), and the recorded holograms result in a nonuniform carrier frequency along the hologram, equivalent to a defocusing in the Fourier transform of the hologram. The defocusing can be compensated by digitally multiplying the recorded hologram by the appropriate spherical phase factor. On the other hand, the scale change produces an outward lateral shift of the position of the pinhole images, and thus the carrier frequencies of the holograms for each source increase. The modification of the carrier frequencies generates an incorrect overlapping of the frequency bands in the spectrum [Fig. 3(b)]. In this situation the reconstruction of the hologram would be wrong. Moreover, a separate processing of every bandpass is not possible due to overlapping. To cope with this problem, the axial shift of the lens (that changes the pinhole mask magnification) can be adjusted such that the frequency bands are not overlapped [Fig. 3(c)].

Thus, the lens placed in the reference beam needs to accomplish two conditions. It must image the exit pupil of the microscope objective onto the CCD to optimize light intensity of the reference. And on the other hand, it must have a magnification that avoids the overlapping of the different frequency bands. Notice that the second condition is only necessary to work in a single exposure, that is, when all the point sources operate simultaneously. Otherwise, if the process is done sequentially, the overlapping does not generate any implementation problem.

3. THEORETICAL SYSTEM ANALYSIS

In this section we review the mathematical foundations of the experimental setup diffraction analysis. Let us first analyze the imaging arm of the system (Fig. 1). An input object $f(x,y)$ will produce a scaled image in the output plane, convolved with the point-spread function (PSF) of the imaging system. We will assume that the CFT of the system is a circular aperture with radius $\Delta\nu$, $\mathrm{circ}(\rho/\Delta\nu)$, ρ being the radius in the spatial-frequency domain. Thus, the PSF is its inverse Fourier transform, related to the first-order Bessel function, that we will denote as $\mathrm{disk}(\Delta\nu r)$, where r is the radial coordinate in the output plane. The complex distribution at the image plane when the object is illuminated by a centered source, under Fresnel approximation, is

$$U(x,y) = \left(f\left(-\frac{x}{M}, -\frac{y}{M} \right) \exp\left\{ j\frac{k}{2d}[x^2+y^2] \right\} \right) \otimes \mathrm{disk}(\Delta\nu r), \tag{1}$$

where (x,y) are the spatial coordinates on the output plane and $k=2\pi/\lambda$ is the wavenumber. Note that the image is scaled according to the image magnification (M) and the phase factor multiplying the image diverges from a distance d from the output plane, that is, from the intermediate image of the source (see Fig. 1).

An $m \times n$ 2D source array is used to illuminate the input object. For a single off-axis source, the only modification is a shift in the spatial coordinates in the quadratic phase factor. Naming (x_m, y_n) the coordinates of VCSEL sources in the source plane, their images in the interme-

diate aerial image will be displaced according to the magnification given by the lens between the source and the source image plane (M_s). Thus for a single source the amplitude distribution on the CCD through the imaging arm of the setup is given by

$$U^I_{m,n}(x,y) = \left(f\left(-\frac{x}{M}, -\frac{y}{M} \right) \times \exp\left\{ j\frac{k}{2d}[(x - M_s x_m)^2 + (y - M_s y_n)^2] \right\} \right) \otimes \mathrm{disk}(\Delta\nu r), \quad (2)$$

where the superscript I stands for the imaging arm and the subscripts give the indices of the source in the array.

Concerning the reference arm of the system (Fig. 2), a single source will give an aerial intermediate image, just as in the imaging arm. In addition, the lens close to the pinhole mask will axially shift and scale the intermediate image. As a whole, the light impinging on the CCD will diverge from a distance d' and a lateral position affected by a magnification $M's$ (both parameters depend on the lens layout in the experimental setup). With a the distance between the mask and the lens and F the focal length of the lens, the distance d' is

$$d' = \frac{a(a-d) + F^2}{F - a}. \quad (3)$$

And the magnification is modified as follows:

$$M'_s = M_s \frac{F}{F - a}. \quad (4)$$

The amplitude distribution incoming onto the CCD from the reference arm for the (m,n) source is

$$U^R_{m,n}(x,y) = \exp\left\{ j\frac{k}{2d'}[(x - M'_s x_m)^2 + (y - M'_s y_n)^2] \right\}. \quad (5)$$

Note that we assume the pupil function of the field lens does not trim the reference beam. An additional linear phase factor, $\exp\{j2\pi Qx\}$, playing the role of a carrier with frequency Q, can be introduced by tilting one of the mirrors in the reference arm.

Thus, the overall amplitude that impinges on the CCD comes from the addition of Eqs. (2) and (5), and it gives the following intensity distribution:

$$I_{m,n}(x,y) = |U^I_{m,n}(x,y) + U^R_{m,n}(x,y)\exp(j2\pi Qx)|^2. \quad (6)$$

Note that the carrier introduced in the x axis is the same for all sources. Equation (6) can be split into four terms: $T_1(x,y), T_2(x,y), T_3(x,y)$, and $T_4(x,y)$.

$$\begin{aligned} I_{m,n}(x,y) &= 1 + |U^I_{m,n}(x,y)|^2 + U^I_{m,n}(x,y)[U^R_{m,n}(x,y)]^* \\ &\quad \times \exp(-j2\pi Qx) + [U^I_{m,n}(x,y)]^* U^R_{m,n}(x,y) e^{j2\pi Qx} \\ &= T_1(x,y) + T_2(x,y) + T_3(x,y) + T_4(x,y). \end{aligned} \quad (7)$$

Equation (7) represents the hologram recorded on the CCD for a single source the centered at the (x_m, y_n) position. In the reconstruction procedure, we perform digitally an inverse Fourier transformation of Eq. (7) to analyze each term separately. The first term, $T_1(x,y) = 1$, is constant and its Fourier transform $[\tilde{T}_1(u,\nu)]$ is just a delta function centered at the origin. The second term, $T_2(x,y)$, is the intensity of a low-pass version of the image as given by the system. Thus, its Fourier transform $[\tilde{T}_2(u,\nu)]$ is also centered at the origin, with a width that doubles the bandpass of the system.

The third and fourth terms in Eq. (7) contain the information about the phase and the amplitude of the object. The third term is

$$\begin{aligned} T_3(x,y) &= \left[\left(f\left(-\frac{x}{M}, -\frac{y}{M} \right) \exp\left\{ j\frac{k}{2d}[(x - M_s x_m)^2 + (y - M_s y_n)^2] \right\} \right) \otimes \mathrm{disk}(\Delta\nu r) \right] \\ &\quad \times \exp\left\{ -j\frac{k}{2d}[(x - M'_s x_m)^2 + (y - M'_s y_n)^2] \right\} \\ &\quad \times \exp(-j2\pi Qx). \end{aligned} \quad (8)$$

The Fourier transform of the third term, $[\tilde{T}_3(u,\nu)]$, is a bandpass of the object spectrum shifted by the carrier frequency Q and placed at the left position of the central autocorrelation term (-1 diffraction order for the holographic recording process).

$$\begin{aligned} \tilde{T}_3(u,\nu) &= K\left[\left(\tilde{f}\left(Mu + \frac{MM_s}{\lambda d} x_m, M\nu + \frac{MM_s}{\lambda d} y_n \right) \otimes \mathrm{FT}^{-1}\left\{ \exp\left[j\frac{k}{2d}(x^2 + y^2) \right] \right\} \right) \mathrm{circ}\left(\frac{\rho}{\Delta\nu} \right) \right] \\ &\quad \otimes \mathrm{FT}^{-1}\left\{ \exp\left[-j\frac{k}{2d'}(x^2 + y^2) \right] \right\} \\ &\quad \otimes \delta\left(u + Q - \frac{M'_s}{\lambda d'} x_m, \nu - \frac{M'_s}{\lambda d'} y_n \right), \end{aligned} \quad (9)$$

where K is a constant that also includes constant phase factors, and $\tilde{f}$ is the Fourier transform of the input. Note that the fourth term in Eq. (7) is the complex conjugate of the third term and has a similar meaning. The last delta function in Eq. (9) has the following meaning: It implies a frequency shift in the transmitted spectral bandpass necessary to guarantee the separation between the -1 diffraction order from the zero order; on the other hand, it implies additionally a slight frequency shift due to the different position of the source in the 2D array (x_m, y_n) affected by the magnification factor M'_s. This fact will be considered below. Now, if we put aside the convolution with delta in Eq. (9), the convolution between the two remaining terms must be analyzed separately. The first one is related to the frequency band of the object spectrum convolved with the Fourier transform of a spherical phase factor and is truncated by the pupil function (circ function) of the microscope objective, i.e., restricted to a circular-limited frequency extension in the Fourier domain. Then this term is convolved with the Fourier transformation of another spherical phase factor, which has no effect outside the limited circular region. Thus, a combi-

nation of the two spherical phase factors is possible inside the pupil extension.

$$\mathrm{FT}^{-1}\left\{\exp\left[j\frac{k}{2d}(x^2+y^2)\right]\right\}\otimes\mathrm{FT}^{-1}\left\{\exp\left[-j\frac{k}{2d'}(x^2+y^2)\right]\right\}$$
$$=\mathrm{FT}^{-1}\left\{\exp\left[j\frac{k}{2d}\left(\frac{1}{d}\frac{1}{d'}\right)(x^2+y^2)\right]\right\}. \quad (10)$$

The combined factor presented in Eq. (10) implies a defocusing inside the limited region defined by the circ function of the corresponding frequency band and has to be removed to perform a correct reconstruction. Note that if the lens could be placed on the mask pinhole plane (acting as a field lens), no defocusing effect would happened. To remove this defocusing, we digitally multiply the recorded hologram by the complex conjugate of the defocusing spherical phase factor in Eq. (10), prior to its Fourier transforming. After removing the defocusing, the third term becomes

$$\tilde{T}'_3(u,v)=K\left\{\tilde{f}\left(Mu+\frac{MM_s}{\lambda d}x_m, Mv+\frac{MM_s}{\lambda d}y_n\right)\mathrm{circ}\left(\frac{\rho}{\Delta\nu}\right)\right\}$$
$$\otimes\,\delta\left(u+Q-\frac{M'_s}{\lambda d'}x_m, v-\frac{M'_s}{\lambda d'}y_n\right). \quad (11)$$

Equation (11) describes the information of the spectral frequency bandpass of the object spectrum transmitted by the pupil microscope objective in the case of one source centered at the (x_m,y_n) position. The carrier frequency Q is controlled by tilting the mirror of the reference beam and permits the separation of the bandpasses from the origin.

Now, if we consider all the illumination sources from the 2D source array, the addition of the refocused third terms gives

$$\tilde{T}'^{\mathrm{sum}}_3(u,v)=K\sum_{m,n}\left\{\left[\tilde{f}\left(M\left(u+\frac{M_s}{\lambda d}x_m\right),\right.\right.\right.$$
$$\left.\left.\left.M\left(v+\frac{M_s}{\lambda d}y_n\right)\right)\mathrm{circ}\left(\frac{\rho}{\Delta\nu}\right)\right]$$
$$\otimes\,\delta\left(u-\frac{M'_s}{\lambda d'}x_m, v-\frac{M'_s}{\lambda d'}y_n\right)\right\}\otimes\delta(u+Q,v). \quad (12)$$

In Eq. (12), the term between square brackets represents different frequency bands of the object spectrum transmitted by the circ function. Those different frequency bands are shifted by means of the convolution operations according to distance d', the magnifying factor M'_s, and the bias carrier frequency Q. Note that the frequency bands are centered at different positions than the displacements introduced by the delta functions. In the case that the lens acts as a field lens, the magnification factors and the axial distances coincide ($M'_s=M_s$ and $d=d'$); then the addition in Eq. (12) can be simplified to

$$\widetilde{T'}^{\mathrm{sum}}_3(u,v)=K\tilde{f}(Mu,Mv)\mathrm{SA}(u,v)\otimes\delta(u+Q,v), \quad (13)$$

where

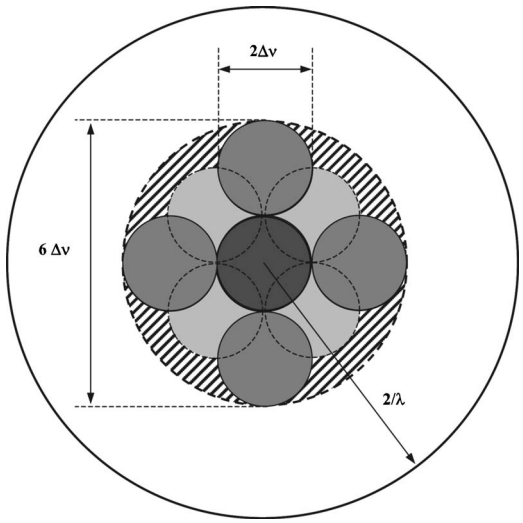

Fig. 4. Synthetic aperture generation by the off-axis illumination used in the present approach. The different gray levels represent the frequency bandpasses. The dashed area shows a full aperture of width $6\Delta\nu$.

$$\mathrm{SA}(u,v)=\sum_{m,n}\mathrm{circ}\left(\frac{u-\frac{M_s}{\lambda d}x_m}{\Delta\nu}, \frac{v-\frac{M_s}{\lambda d}y_m}{\Delta\nu}\right). \quad (14)$$

Equation (14) represents a synthetic aperture, obtained by adding the shifted versions of the circular aperture of the system, analogously to Fig. 3(a). In practice, for the experimental parameters that we have used, the term $\tilde{T}'^{\mathrm{sum}}_3(u,v)$ gives a first diffraction order frequency distribution similar to the representation of Fig. 3(c); by performing a digital stage of filtering and relocation of the different frequency bands it would be possible to obtain all terms overlapping at the desired locations yielding the generation of the desired synthetic aperture. Moreover, digital processing is not time-consuming, as it involves only linear and simple calculations.

Nevertheless, to simplify the setup and to show the capabilities of the presented approach, we have used a laser as a point source and moved it to the off-axis positions sequentially. By the arrangement of the different frequency bands in a second stage, the synthetic aperture is performed digitally and is depicted in Fig. 4. The size of the smallest circles corresponds to the NA of the microscope objective ($\Delta\nu$ radius). The desired synthetic pupil (dashed circle line of $6\Delta\nu$ diameter approximately) is almost covered by a set of elemental apertures. The on-axis illumination pupil (dark gray in Fig. 4) is complemented with eight additional shifted apertures. Four of them are accomplished by source shifts in (X,Y) orthogonal directions (medium gray level in Fig. 4). The other four pupils are obtained by off-axis illuminations for each oblique direction (light gray level in Fig. 4). The actual cutoff frequency is increased to three times the conventional cutoff frequency of the microscope objective, resulting in a notable resolution enhancement when an inverse Fourier transformation is done to recover the superresolved object.

One important advantage of this new superresolution system, in comparison with those systems developed pre-

viously by us in Refs. 28 and 31, is, aside from the possibility of obtaining a superresolution effect for a 2D object in a single exposure, that the interferometric process is performed after the imaging system. Thus, the system shows an easy and simplified configuration that may be adapted for any practical microscopy systems because the interferometric setup is located between the microscope lens and the CCD.

Further advantages are related to the possibility of working not only for real-valued objects but also for complex or phase objects. Note that no assumption about the properties of the amplitude object $f(x,y)$ is made; so for any complex input distribution, the reconstruction of the input may be obtained.

4. EXPERIMENTAL RESULTS

For the new proposed superresolution method we have used a 2D array source that consists of a point laser source with the possibility of lateral displacement. We have used a Nikon microscope objective with a NA of 0.1 and 5× magnification. Note that a large working distance, as needed for many practical applications, is usually related to a low NA. A 532 nm wavelength laser is used as illumination. The laser beam is spatially filtered providing the point source necessary for the experiments and it is placed onto a motorized mechanical platform to obtain the off-axis illuminations in a sequential mode. In addition to the on-axis illumination, we have carried out eight off-axis illuminations, as depicted in Fig. 4. The input object is a negative 1951 U.S. Air Force high-resolution test. The microscope objective, as given by its NA, has a resolution spot size of 4.9 μm, which approximately corresponds to group 7, element 5 resolution in the test target, when coherent illumination is used. This situation is shown in Fig. 5 where the low-resolution image obtained with the 0.1 NA objective is compared with a high-resolution image done by a Spindler & Hoyer microscope objective with a 0.65 NA. The high-resolution image is taken as a reference and it is captured at very different imaging conditions (magnification, working distance, etc.,). Clearly, many spatial frequencies are not transferred by the low-NA objective and a low-pass version of the object test is obtained.

Then we perform the superresolving approach using the recording of eight off-axis holograms and store this in the computer memory. Taking into account the 0.1 NA of the lens, four exposures along the X and Y axes are made by shifting the source 11.5 deg with respect to the optical axis. The four diagonal bandpasses require an angle of 5.75 deg on both the X and Y axes. Although the process is done sequentially, Fig. 6 depicts the image addition of the nine recorded holograms in the Fourier transformation (eight off-axis illuminations and one on-axis case) showing the ability of the present approach to work in one step when a pinhole mask is used. Note that the different frequency bands are nonoverlapping due to the proper adjustment of the reference arm lens. A lens ($f' = 100$ mm) attached to the pinhole mask in the reference arm is used. A spherical phase factor [see Eq. (6)] has been multiplied to each recorded hologram to focus the −1 order. However, because the lens in the experimental setup is placed close to the pinhole mask, the defocusing effect is almost negligible. Note that the carrier frequency has been shifted from zero (tilting the reference mirror) to separate the spatial-frequency slot from the zero-order terms.

By a simple digital postprocessing operation, each of the frequency bands of the −1 diffraction order is shifted to the correct spectral positions and then all of them are superimposed to synthesize the desired synthetic aper-

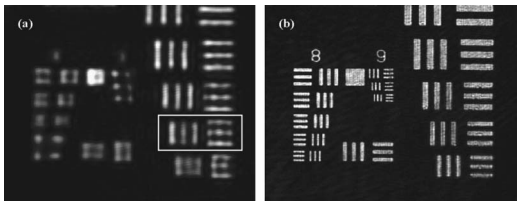

Fig. 5. (a) Image obtained with the 0.1 NA objective lens and coherent illumination. (b) High-resolution image obtained with a Spindler & Hoyer microscope objective with a 0.65 NA and coherent illumination. Note that the resolution limit corresponds to the rectangle shown in (a) and it implies a cutoff frequency of 203.0 line pairs/mm (group 7, element 5), which means a smallest resolved detail of 4.93 μm.

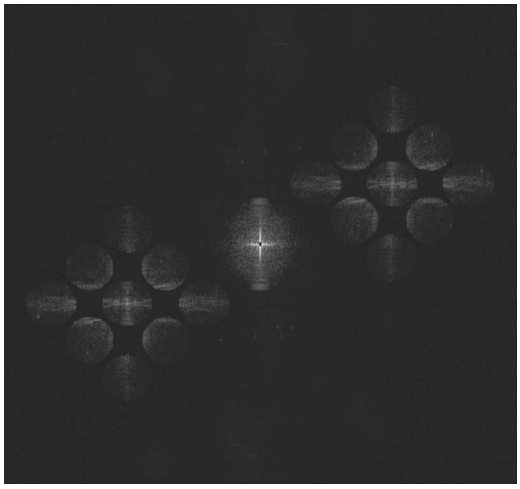

Fig. 6. Fourier transform of the addition of different recorded holograms. The dc has been blocked to improve contrast.

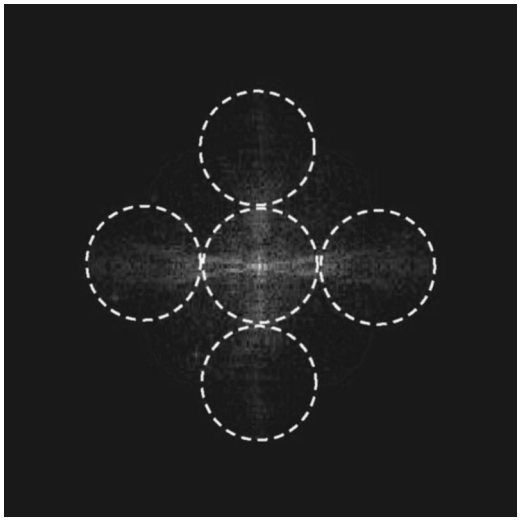

Fig. 7. Resulting synthetic aperture.

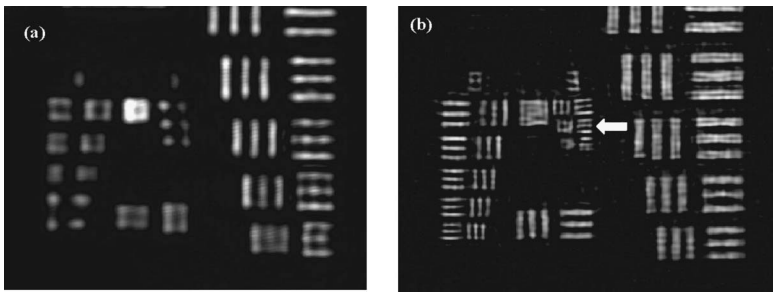

Fig. 8. (a) Image obtained with 0.1 NA lens and conventional illumination. (b) Superresolved image obtained with the synthetic aperture. The group 9, element 2 corresponding to the resolution limit using the proposed method is marked with an arrow.

ture. An inverse Fourier transform yields the final superresolved image. Figure 7 shows the generated synthetic aperture where five of the partial bandpasses have been marked with dashed circles for clarity. According to theory, the resolution has been enhanced by a factor of 3 in both the horizontal and the vertical directions and by a factor of 2.4 in the oblique directions. As a consequence, the resolution spot size is reduced until it is 1.64 μm for the horizontal and vertical directions, which approximately corresponds to the resolution limit given by group 9, element 2 of the resolution test target (575.0 line pairs/mm frequency cutoff, 1.74 μm resolution limit). So the resolution improvement implies a synthetic aperture of approximately 0.32 synthetic NA. Figure 8 shows a comparison between the image with the 0.1 NA objective lens used in the conventional imaging [Fig. 8(a)], and with the suggested superresolving approach [Fig. 8(b)]. It is evident that the improvement of resolution and the resolution expected from the theoretical calculations are effectively obtained.

5. CONCLUSIONS

In this paper we have presented a superresolving approach for digital holographic microscopy where the superresolution effect is described in terms of a synthetic aperture generation. The basic idea is to superimpose multiple digital image holograms obtained using different illumination point sources. Although the approach is demonstrated experimentally by shifting a single point source in sequential mode, the system can work in a single-exposure approach using the illumination produced by a 2D array of mutually incoherent sources. Thus, each shifted illumination beam generates a shift in the object spectrum in such a way that different spatial-frequency bands are transmitted through the objective lens. An interferometric setup after the microscope objective allows the holographic recording process for each transmitted frequency band. An improvement resolution factor of 3 is achieved, in comparison with the resolution of the tested microscope objective for a standard configuration.

One of the main advantages of our method is the possibility of recording all the holograms at once without any changes in the optical setup. The system, as compared with previous setups, is simple and robust because the interferometric system is placed after the imaging lens and the whole process is done on the image space. The approach does not require a high degree of temporal coherence for the illumination system because the interferometric imaging setup can be adjusted close to zero path difference; thus, low temporal coherent sources, such as diodes arrays and high-powered VCSEL arrays with low spatial coherence, can be used as illumination sources.

ACKNOWLEDGMENTS

This work was supported by Fondo Europeo de Desarrollo Regional funds and the Spanish Ministerio de Educación y Ciencia under project FIS2004-06947-C02-01.

The e-mail address for J. García is javier.garcia.monreal@uv.es.

REFERENCES

1. W. S. Haddad, D. Cullen, J. C. Solem, J. W. Longworth, A. McPherson, K. Boyer, and C. K. Rhodes, "Fourier-transform holographic microscope," Appl. Opt. **31**, 4973–4978 (1992).
2. U. Schnars and W. P. O. Jüpter, "Direct recording of holograms by a CCD target and numerical reconstruction," Appl. Opt. **33**, 179–181 (1994).
3. S. Grilli, P. Ferraro, S. De Incola, A. Finizio, G. Pierattini, and R. Meucci, "Whole optical wavefields reconstruction by digital holography," Opt. Express **9**, 294–302 (2001).
4. U. Schnars, "Direct phase determination in hologram interferometry with use of digitally recorded holograms," J. Opt. Soc. Am. A **11**, 2011–2015 (1994).
5. A. Decker, Y. Pao, and P. Claspy, "Electronic heterodyne recording and processing of optical holograms using phase modulated reference waves (*T*)," Appl. Opt. **17**, 917–921 (1978).
6. I. Yamaguchi and T. Zhang, "Phase-shifting digital holography," Opt. Lett. **22**, 1268–1270 (1997).
7. P. Guo and A. J. Devaney, "Digital microscopy using phase-shifting digital holography with two reference waves," Opt. Lett. **29**, 857–859 (2004).
8. I. Yamaguchi, J.-I. Kato, S. Otha, and J. Mizuno, "Image formation in phase-shifting digital holography and applications to microscopy," Appl. Opt. **40**, 6177–6186 (2001).
9. T. Zhang and I. Yamaguchi, "Three-dimensional microscopy with phase-shifting digital holography," Opt. Lett. **23**, 1221–1223 (1998).
10. S. Lai and M. A. Neifeld, "Digital wavefront reconstruction and its application to image encryption," Opt. Commun. **178**, 283–289 (2000).
11. S. Lai, B. King, and M. A. Neifeld, "Wave front reconstruction by means of phase-shifting digital in-line holography," Opt. Commun. **173**, 155–160 (2000).
12. F. Le Clerc, M. Gross, and L. Collot, "Synthetic aperture experiment in the visible with on-axis digital heterodyne holography," Opt. Lett. **26**, 1550–1552 (2001).
13. J. H. Massig, "Digital off-axis holography with a synthetic aperture," Opt. Lett. **27**, 2179–2181 (2002).

14. Z. Zalevsky and D. Mendlovic, *Optical Super Resolution* (Springer, 2002).
15. Z. Zalevsky, D. Mendlovic, and A. W. Lohmann, "Optical systems with improved resolving power," in *Progress in Optics, Vol. XL*, E. Wolf, ed. (Elsevier, 1999), Chap. 4.
16. G. Toraldo di Francia, "Resolving power and information," J. Opt. Soc. Am. **45**, 497–501 (1955).
17. G. Toraldo di Francia, "Degrees of freedom of an image," J. Opt. Soc. Am. **59**, 799–804 (1969).
18. I. J. Cox and J. R. Sheppard, "Information capacity and resolution in an optical system," J. Opt. Soc. Am. A **3**, 1152–1158 (1986).
19. W. Lukosz, "Optical systems with resolving powers exceeding the classical limit. II," J. Opt. Soc. Am. **57**, 932–941 (1967).
20. A. Shemer, D. Mendlovic, Z. Zalevsky, J. Garcia, and P. García-Martínez, "Superresolving optical system with time multiplexing and computer decoding," Appl. Opt. **38**, 7245–7251 (1999).
21. P. C. Sun and E. N. Leith, "Superresolution by spatial–temporal encoding methods," Appl. Opt. **31**, 4857–4862 (1992).
22. M. Françon, "Amélioration de la reśolution d'optique," Nuovo Cimento, Suppl. **9**, 283–290 (1952).
23. A. W. Lohmann and D. P. Parish, "Superresolution for nonbirefringent objects," Appl. Opt. **3**, 1037–1043 (1964).
24. A. Zlotnik, Z. Zalevsky, and E. Marom, "Superresolution with nonorthogonal polarization coding," Appl. Opt. **44**, 3705–3715 (2005).
25. A. I. Kartashev, "Optical system with enhanced resolving power," Opt. Spectrosc. **9**, 204–206 (1960).
26. X. Chen and S. R. J Brueck, "Imaging interferometric lithography: approaching the resolution limits of optics," Opt. Lett. **24**, 124–126 (1999).
27. C. J. Schwarz, Y. Kuznetsova, and S. R. J. Brueck, "Imaging interferometric microscopy," Opt. Lett. **28**, 1424–1426 (2003).
28. V. Mico, Z. Zalevsky, P. García-Martinez, and J. García, "Single step superresolution by interferometric imaging," Opt. Express **12**, 2589–2596 (2004).
29. E. N. Leith, D. Angell, and C.-P. Kuei, "Superresolution by incoherent-to-coherent conversion," J. Opt. Soc. Am. A **4**, 1050–1054 (1987).
30. E. N. Leith, "Small-aperture, high-resolution, two-channel imaging system," Opt. Lett. **15**, 885–887 (1990).
31. V. Mico, Z. Zalevsky, P. García-Martínez, and J. García, "Superresolved imaging in digital holography by superposition of tilted wavefronts," Appl. Opt. **45**, 822–828 (2006).
32. C. J. R. Sheppard and Z. Hegedus, "Resolution for off-axis illumination," J. Opt. Soc. Am. A **15**, 622–624 (1998).
33. M. G. L. Gustafsson, "Surpassing the lateral resolution limit by a factor of two using structured illumination microscopy," J. Microsc. **198**, 82–87 (2000).